High radiation scenarios with radiation inside the confined region at ASDEX Upgrade

M. Bernert[1], F. Reimold[1,2], R. Dux[1], T. Eich[1], S. Glöggler[1], A. Kallenbach[1], B. Lipschultz[3], M. Wischmeier[1], the EUROfusion MST1 team* and the ASDEX Upgrade team

[1]Max-Planck-Institut für Plasmaphysik, Boltzmannstraße 2, 85748 Garching, Germany
[2]Forschungszentrum Juelich GmbH, Wilhelm-Johnen-Straße, 52425 Juelich, Germany
[3]University of York, York Plasma Institute, Heslington, York, YO1 9DD, United Kingdom

Introduction

For future reactors, plasma scenarios with high radiated power fractions are required to reduce the power flux to the divertor target plates. While for ITER about 85-90% of the exhaust power has to be dissipated, for DEMO more than 95% are required to meet the material limits. The power dissipation consists of perpendicular transport, charge exchange losses and radiation losses, the latter being the biggest contribution [1, 2]. The radiated power can be increased by introducing seed impurities. These can be chosen to increase primarily the core (e.g. Kr, W) or scrape-off-layer radiation (e.g. N, Ne). To retain the enhanced energy confinement of the H-mode, the power flux across the separatrix has to stay above the H-L threshold. Therefore, at ITER additional radiation in the core is not feasible, while for DEMO the expected excess of alpha heating above the H-mode threshold allows (and requires) significant core radiation. [3]

High radiation scenarios at ASDEX Upgrade

High radiation scenarios are investigated at the fully tungsten covered ASDEX Upgrade tokamak (AUG). These include divertor and core radiation, e.g. the double radiative feedback as demonstrated in [4]. In 2014, a pronounced detachment [5] of the outer target was achieved at highest heating powers ($P_{heat}/R \approx 13\,\mathrm{MW/m}$). In these scenarios up to 17 MW of neutral beam heating, 4 MW ion cyclotron resonance heating and 1 MW of electron cyclotron resonance heating (in O-2 mode) was applied. Significant central microwave heating is required to avoid the accumulation of tungsten. To facilitate detachment and mitigate magnetic modes, a neutral gas pressure of more than 2 Pa is required, which is achieved by reducing the cryo pump capacity. The divertor detachment is induced by intense impurity seeding of either krypton or nitrogen. With Kr about 75% of the heating power is radiated. With N seeding it is possible to achieve a radiated fraction of about 90%. These two scenarios are discussed here.

Predominant edge radiation (N seeding)

The pronounced divertor detachment can be achieved at heating powers of about 20 MW with intense seeding of nitrogen ($\Gamma_N \geq 1.5 \cdot 10^{22} e^-/s$). Figure 2 shows the tomographic reconstructions of the radiation before and during the detached phase of discharge AUG #30506 (see also Fig. 1a). A poloidally strongly localized radiator around the X-point evolves with the detachment. Despite this radiator, the plasma is in a quasi-stable regime (withstanding ELMs and trips of heating power), unlike in the operation with carbon as first wall material [6].

*See http://www.euro-fusionscipub.org/mst1.

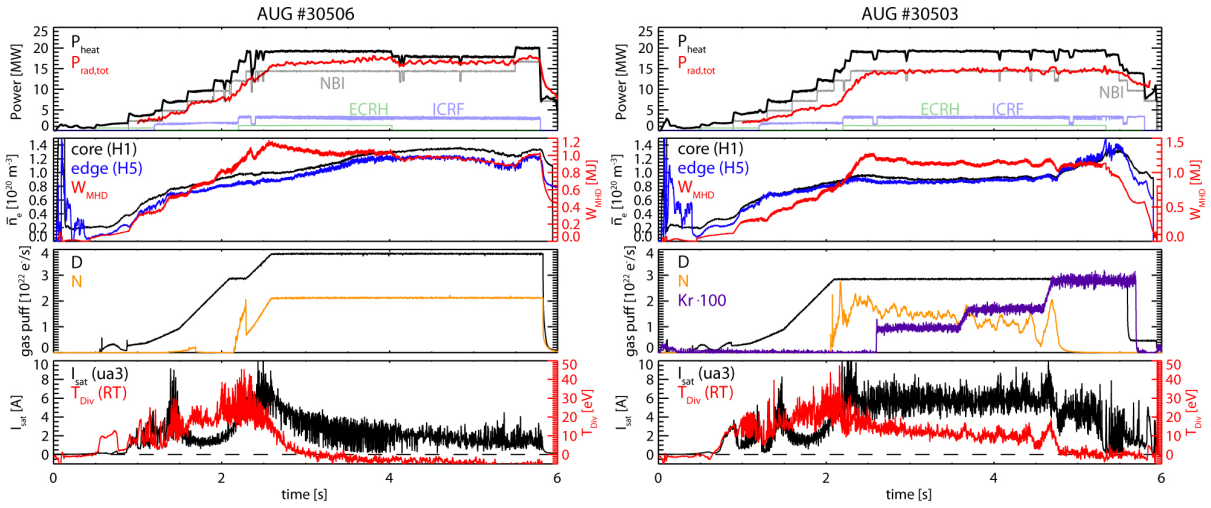

(a) Only N seeding (b) Kr seeding (stepwise replacing N seeding)

Figure 1: Time traces of two high radiation discharges.

In the presented discharge, a constant N puff leads to a slow increase of the central N concentration ($c_N = 2\% \rightarrow 2.5\%$). With this evolution, the X-point radiator moves upwards inside the confined region. The time scale of this evolution is around 2 s.

When the X-point radiator moved significantly inside the confined region, intense deuterium line radiation can be observed in the region between the X-point and the radiator. This indicates electron temperatures (T_e) in the range of a few eV and high neutral densities inside the confined region. The pedestal top T_e is reduced to about $400-500$ eV [7]. The T_e measured in the midplane and the observation of deuterium line radiation at the X-point suggest the presence of parallel T_e gradients. Such gradients combined with a X-point radiator were also reproduced by SOLPS modeling [7].

The reduction of pedestal top temperature does only marginally affect the overall confinement, as the pressure stays constant within $\rho_{pol} < 0.8$ [8]. Thus, the (volume integrated) energy confinement time is reduced by about 10% in comparison to the attached case, whereas the core pressure is not affected.

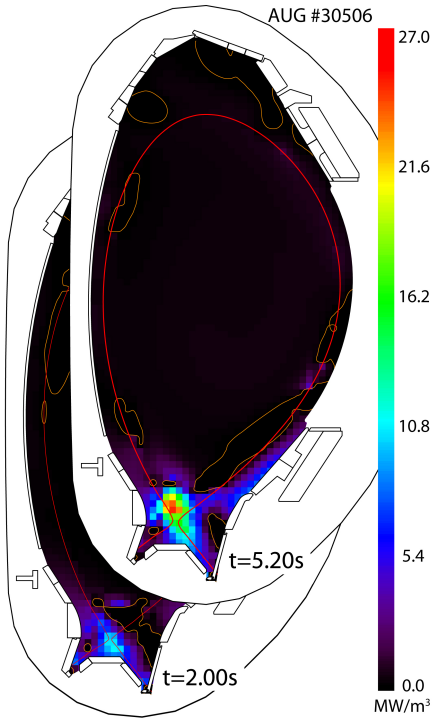

Figure 2: Evolution of the radiation for N induced detachment

Predominant core radiation (Kr seeding)

Krypton radiates predominantly at electron temperatures of about $300-500$ eV. Thus, it is mainly radiating in the pedestal region for standard scenarios at AUG.

Figure 1b shows a discharge, where Kr is step-wise substituting the (feedback-controlled) N. At the first two Kr levels, the plasma parameters change only marginally, Kr is compensating the effects of N (i.e. total radiated power, impact on confinement). At the highest seeding level ($\Gamma_{Kr} = 3 \cdot 10^{20} e^-/s$) a radiating ring in the pedestal region comes up (see Fig. 3).

The power flux into the divertor is reduced, the outer divertor detaches. This nonlinear response of the plasma on the Kr seeding indicates a radiation condensation: If sufficient Kr is present in the pedestal, it cools down the plasma to temperatures where Kr radiates more efficiently. By a density increase, which is regularly observed at the detachment, the pedestal radiation is even further increased.

Such a radiation condensation is observed to either keep the confinement constant for several energy confinement times (AUG #30503, $P_{heat} \approx 19$ MW) or reduce it (e.g. AUG #31645 & #31648, $P_{heat} \approx 10.5$ MW). The different responses of the plasma depend most likely on the resulting temperature profile and the dominant radiation location of Kr. The change of the radiation profiles before and after the radiation condensation (see Fig. 4) show that at a higher heating power, the dominant Kr radiation stays in the pedestal region, while in the lower heated discharges, the radiation moves further inside the confined region. In the first case, the temperature reduction is compensated by a density increase. At lower heating power, the density only changes marginally, leading to the reduced confinement.

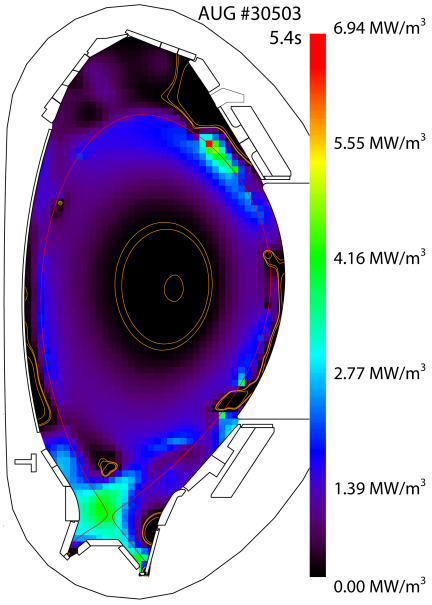

Figure 3: Reconstruction of total radiation in case of Kr induced detachment

ELM transport: The pedestal radiation with Kr is strongly influenced by ELMs. Measurements of AXUV diodes mainly observing the pedestal or the scrape-off layer (SOL) radiation at the beginning of Kr seeding are shown in Figure 5. The pedestal radiation increases with the Kr seeding but is strongly modulated by ELMs. Kr is transported into the pedestal in between ELMs and flushed out by ELMs [10]. The absence of some ELMs and the resulting strong increase of the pedestal radiation indicate a potential runaway situation. Therefore, high frequent ELMs are required to remain in a quasi-stable operation.

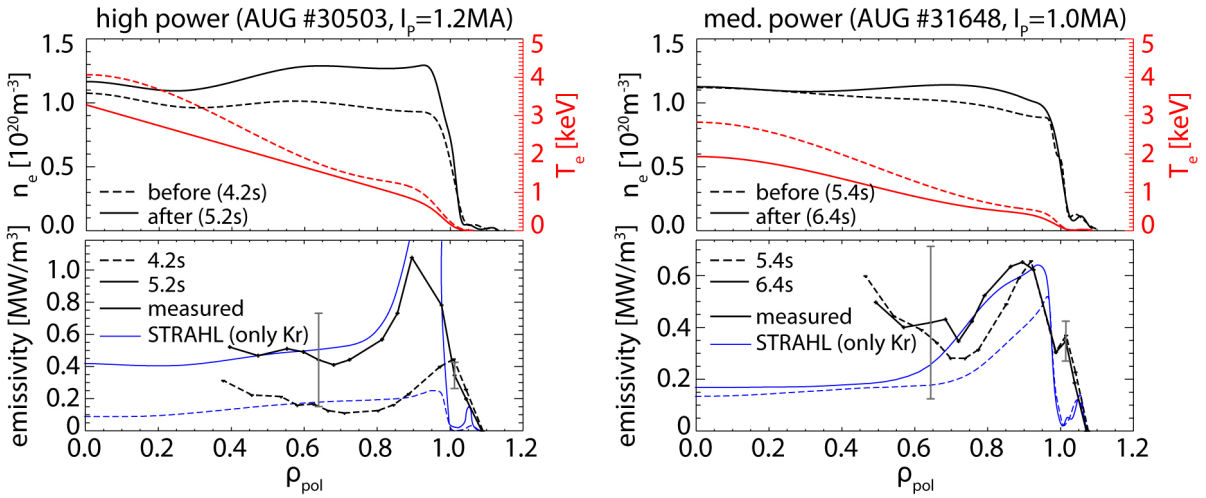

Figure 4: Density and temperature profiles and emissivity (measured by bolometry or simulated with STRAHL [9]) of two Kr seeded discharges before and after the radiation condensation.

The ELM frequency is reducing with increasing Kr radiation. This is in line with the type-I ELM frequency dependency on the heating power or the power flux over the separatrix [11], respectively. At the time of the radiation condensation, the ELM frequency drops drastically, which might lead to an unstable regime. However, at the same time the ELM type changes (most likely type-III), the ELM frequency increases and the plasma is back in a quasi-stable operation.

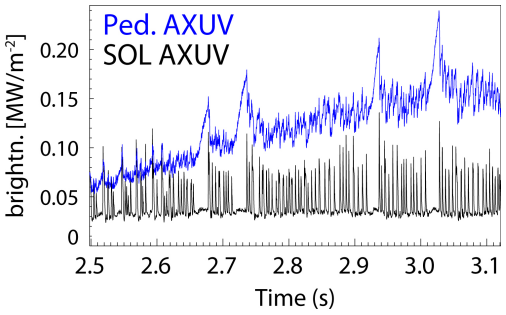

Figure 5: Influence of ELMs on pedestal radiation in presence of Kr.

Discussion

For both scenarios (N or Kr seeding), the dominant radiation originates in the detached state from the confined region. While this is expected from krypton, the radiative loss parameter L_z of nitrogen would suggest dominant divertor radiation. Hence, the radiation has for both scenarios a strong impact on the plasma parameters, resulting in the radiation condensation. The latter can occur due to a negative temperature dependence of L_z. The radiation condensation is for N poloidally localized above the X-point, where radiation losses compete with parallel heat conduction [12]. For Kr this condensation occurs more symmetrically distributed around the pedestal top and perpendicular heat transport must play an important role. Both scenarios are comparable to poloidally detached plasmas [12], reducing significantly the divertor heat load.

The presented scenarios were not yet operated in a steady-state condition. The long term stability is not shown, but both scenarios are stable versus transients, such as ELMs or beam trips. Further development and advanced control might be necessary. In case of the N seeded discharge, real-time algorithms, which control the position of the X-point radiator, should be feasible. The time scale of the evolution of the discharge (~2 s) is much slower than the typical transport times of the nitrogen into the pedestal (~ 50 - 100 ms). For Kr seeding the ELM behaviour plays an important role and further experiments are required.

Outlook

The presented experiments demonstrate possible exhaust scenarios at reactor relevant values of P_{heat}/R. The optimal impurity mix has to be found in order to increase the fusion gain. While for current experiments, N and Kr are be adequate impurities to create the required radiation pattern, future experiments might have to use other impurities, e.g. xenon. However, the observations presented here highlight, that the intricate response of the plasma on the radiation has to be taken into account.

Acknowledgement

This work has been carried out within the framework of the EUROfusion Consortium and has received funding from the Euratom research and training programme 2014-2018 under grant agreement No 633053. The views and opinions expressed herein do not necessarily reflect those of the European Commission.

References

[1] M. Wischmeier et al, J. Nucl. Mat. **463**, 22 (2015) and references therein
[2] A. S. Kukushkin et al, J. Nucl. Mat. **438**, S203 (2013)
[3] H. Zohm et al, Nucl. Fusion **53**, 073019 (2013)
[4] A. Kallenbach et al, Nucl. Fusion **52**, 122003 (2012)
[5] A. Kallenbach et al, Nucl. Fusion **55**, 053026 (2015)
[6] J.A. Wesson et al., Nucl. Fusion **29**, 641 (1989)
[7] F. Reimold et al, J. Nucl. Mat. **463**, 128 (2015)
[8] F. Reimold et al, Nucl. Fusion **55**, 033004 (2015)
[9] R. Dux, STRAHL, annual IPP report **10/30** (2006)
[10] R. Dux et al, Nucl. Fusion **51**, 053002 (2011)
[11] H. Zohm et al, Plasma Phys. Control. Fusion **38**, 105 (1996)
[12] B. Lipschultz et al, Phys. Rev. Letters **81**, 1007 (1998) and references therein